Article citation info:
Raouf EA. Injection timing – driven redistribution of combustion intensity and pressure-induced mechanical loading in a turbocharged diesel engine. Combustion Engines. 0000;XXX(X):xx-xx. https://doi.org/10.19206/CE-222702

Eihab A. RAOUF

Combustion Engines
Polish Scientific Society of Combustion Engines

Injection timing – driven redistribution of combustion intensity and pressure-induced mechanical loading in a turbocharged diesel engine

ARTICLE INFO

Received: 23 May 2025
Revised: 4 July 2026
Accepted: 17 July 2026
Available online: 3 August 2026

Injection timing effects on combustion intensity redistribution and pressure-induced mechanical loading were evaluated for a turbocharged diesel engine using a calibrated Diesel-RK simulation model. Engine simulations were performed at multiple load conditions with systematic variation of injection timing. Advancing injection timing shifted combustion toward top dead center, accelerating pressure development and increasing the maximum pressure rise rate from approximately 1.2–1.6 bar/°CA to values exceeding 5 bar/°CA under advanced conditions. The maximum piston gas force increased from 55–70 kN to over 100 kN at high load. The results demonstrated that mechanical loading depended on both pressure magnitude and pressure-development rate, indicating a coupled combustion–pressure interaction rather than a single-parameter response. The results showed that mechanical loading depended on both pressure magnitude and pressure-rise behaviour rather than on a single pressure parameter. Increasing pressure-rise rate intensified piston gas-force response, particularly under advanced injection and high-load operation. The results also indicated that combustion-optimal injection timing did not necessarily correspond to mechanically favourable operating conditions.

Key words: *injection timing, combustion–pressure coupling, pressure-rise dynamics, turbocharged diesel engine*

1. Introduction

Diesel engines operating with compression ignition remain the preferred choice for many heavy-duty transport and power-generation applications, largely because they combine efficient fuel conversion with dependable performance across a broad range of operating conditions [1]. The timing of fuel injection is one of the calibration parameters that most directly affects combustion behavior [2]. Advancing or retarding the fuel injection tends to shift the combustion timing with respect to top dead center, which affects the in-cylinder pressure history and the rate at which pressure builds during combustion [3].

Changes in cylinder pressure provide a direct indication of how combustion develops throughout the engine cycle and of the mechanical loads experienced by engine components [4]. The maximum cylinder pressure represents the highest load transferred through the piston, connecting rod, and crankshaft, while the pressure rise rate describes how rapidly this load is generated during combustion [5]. As a result, the choice of injection timing affects both engine performance and emissions, as well as the magnitude and characteristics of the resulting mechanical loading [6].

In conventional engine calibration, limits on peak cylinder pressure and pressure rise rate are applied to ensure mechanical reliability [7]. These limits are generally considered design constraints rather than responses to changes in the combustion process [8]. Different injection timings result in distinct combustion patterns and cylinder pressure traces [9]. As a result, the resulting mechanical loading is determined by the combustion process rather than treated as an independent operating constraint [10].

Despite extensive research on injection timing effects, the relationship among combustion intensity, pressure development, and mechanical loading remains poorly understood across different operating conditions. The present study evaluates combustion intensity and pressure-based loading behavior under variations in injection timing using pressure-derived indicators and operating-condition mapping.

2. Literature review

Injection timing has been examined extensively in experimental studies and numerical simulations [11]. The reported results usually describe changes in ignition delay, heat release rate, peak cylinder pressure, pressure rise rate, fuel consumption, and nitrogen oxide emissions [12]. Earlier fuel injection generally produced stronger premixed combustion and higher cylinder pressure [13]. When injection was delayed, pressure developed more gradually, while thermal efficiency declined [14].

Peak cylinder pressure and maximum pressure rise rate are widely used as calibration constraints because they reflect combustion severity and mechanical loading [15]. These parameters define the acceptable operating range to limit structural loading and combustion noise [16]. Most previous studies assessed engine operation by comparing the calculated values with these limits.

However, in most cases, combustion development and mechanical constraints are treated separately. Previous investigations characterized combustion intensity using heat release or efficiency-based measures [17]. Peak pressure and pressure rise rate were typically considered calibration limits rather than variables linked to combustion development. Consequently, the effect of injection timing on the redistribution of combustion intensity and the associated pressure-induced loading has not been systematically evaluated [18].

Previous research has investigated diesel combustion under different injection strategies and operating conditions [19–21]. Most of these studies evaluated combustion characteristics and stability, whereas the associated pressure loading received less attention. Their analyses were generally limited to individual operating conditions, making it difficult to describe the overall response to changes in injection timing. Consequently, the transition from moderate to severe combustion could not be identified consistently from pressure-based measurements.

This work examines the influence of injection timing on combustion intensity and the associated pressure-induced mechanical loading. Pressure-derived indicators are used to evaluate the evolution of combustion and pressure development under different operating conditions. The analysis identifies load-dependent trends in the pressure response over the investigated injection timing range.

4. Novelty and contribution

The present study evaluates the relationships among combustion intensity, pressure-rise response, and mechanical loading under injection timing variations using pressure-based indicators. Unlike conventional approaches that rely mainly on peak cylinder pressure, the analysis considers both pressure magnitude and pressure-rise response during combustion development.

The analysis also considers the influence of engine load under different injection-timing conditions to distinguish operating regions associated with favorable performance characteristics from those characterized by elevated mechanical loading. The novelty of the present work lies in the combined interpretation of combustion intensity and pressure-based loading response across different operating conditions.

4. Materials and methods

4.1. Engine model, operating conditions and injection strategy

Simulations were performed in Diesel-RK for a turbocharged four-cylinder diesel engine under steady-state conditions. Engine geometry, turbocharging parameters, and boundary conditions were taken from manufacturer data and a validated calibration dataset (Appendix Table A1). The model was calibrated at the rated peak-torque condition (1600 rpm) by adjusting the injected fuel mass per cycle until the predicted brake torque matched 480 N·m. Using a compressor pressure ratio of PR = 1.33 and SOI = 8° bTDC, a fuel quantity of approximately 0.1059 g/cycle produced a torque of about 482 N·m, indicating close agreement with the target condition. The operating matrix was constructed over five engine speeds (1000, 1500, 2000, 2500, and 3000 rpm) and four load levels (25%, 50%, 75%, and 100%), resulting in 120 steady-state simulation cases (5 × 4 × 6). For each speed–load combination, injection timing (SOI) was varied from 0° to 20°CA bTDC in 4°CA increments.

During each injection timing sweep, the injected fuel quantity, injection pressure, and boundary conditions were held constant, and only the injection timing was varied. The recorded outputs included peak cylinder pressure (p_{max}), maximum pressure rise rate ($(dp/d\theta)_{max}$), IMEP, brake power, torque, BSFC, and NO_x emissions.

4.2. Combustion intensity and mechanical loading indicators

Combustion behavior and mechanical loading were characterized using pressure-derived indicators obtained from the in-cylinder pressure trace. The maximum pressure rise rate $(dp/d\theta)_{max}$, was used as a measure of combustion intensity, representing the rate of pressure development during the premixed combustion phase. Peak cylinder pressure (p_{max}) was used to represent the maximum thermodynamic loading acting on the piston–connecting rod–crankshaft system.

The loading response was analyzed as a function of injection timing to identify operating regions where small phasing variations resulted in significant increases in pressure gradients or peak pressure.

4.3. Mathematical formulation of combustion intensity and mechanical loading metrics

The apparent heat release rate (aHRR) was calculated using the first law of thermodynamics as:

$$\frac{d\dot{Q}_{app}}{d\theta} = \frac{\gamma}{\gamma-1} p \frac{dV}{d\theta} + \frac{1}{\gamma-1} V \frac{dp}{d\theta} \quad (1)$$

The pressure rise rate was determined numerically as:

$$\frac{dp}{d\theta} \approx \frac{p_{i+1}-p_i}{\theta_{i+1}-\theta_i} \quad (2)$$

where: p_i and p_{i+1} represent consecutive pressure values at crank angles θ_i and θ_{i+1}, respectively. Combustion phasing (CA50) was defined as:

$$\frac{\int_{SOC}^{CA50} \dot{Q}_{app} d\theta}{\int_{SOC}^{EOC} \dot{Q}_{app} d\theta} = 0.5 \quad (3)$$

where EOC denotes the end of combustion. The mechanical loading index (MLI) was defined as the product of maximum in-cylinder pressure and maximum pressure-rise rate to represent combined pressure magnitude and loading severity:

$$MLI_{raw} = p_{max} \left(\frac{dp}{d\theta}\right)_{max} \quad (4)$$

The raw MLI values were normalized using min–max scaling before their incorporation into the Balanced Score formulation.

$$MLI_{norm} = \frac{MLI_{raw}-MLI_{min}}{MLI_{max}-MLI_{min}} \quad (5)$$

The combustion intensity index (CII) was defined to characterize the temporal concentration of heat release by relating the peak heat-release rate to the combustion duration:

$$CII_{raw} = \frac{HRR_{max}}{(CA95-CA05)} \quad (6)$$

where HRR_{max} denotes the maximum net heat-release rate:

$$HRR_{max} = \left(\frac{dQ}{d\theta}\right)_{max} \quad (7)$$

CA05, CA50, and CA95 correspond to 5%, 50%, and 95% cumulative heat release, respectively. CA05 was adopted as the combustion-onset indicator. The CII values were normalized using min–max scaling according to:

$$CII_{norm} = \frac{CII_{raw}-CII_{min}}{CII_{max}-CII_{min}} \quad (8)$$

The analysis was based on a single-zone thermodynamic model assuming spatially uniform thermodynamic properties within the cylinder. Heat transfer, blow-by, and related losses were incorporated within the apparent heat-release formulation.

4.4. Performance normalization and evaluation criteria

To enable consistent comparison across operating conditions, performance parameters were normalized using a min–max scaling approach as:

$$X^* = \frac{X - X_{min}}{X_{max} - X_{min}} \quad (9)$$

where X_{min} and X_{max} represent the minimum and maximum values over the complete simulation dataset. The normalized evaluation parameters consisted of brake thermal efficiency (BTE*), brake power (BP*), and brake specific fuel consumption (BSFC*). BTE* and BP* were treated as performance-enhancing parameters, whereas BSFC* was minimized. The normalized brake specific fuel consumption was defined as:

$$BSFC^* = 1 - \frac{BSFC - BSFC_{min}}{BSFC_{max} - BSFC_{min}} \quad (10)$$

An aggregated performance score was introduced as:

$$Perf_{Score} = \frac{BTE^* + BP^* + BSFC^*}{3} \quad (11)$$

The performance score ($Perf_{Score}$) was used for comparative evaluation across operating conditions. To evaluate the operating conditions by simultaneously considering performance characteristics and mechanical loading severity, a balanced score was introduced as follows:

$$\text{Balanced Score} = 0.6\, Perf_{Score} + 0.4(1 - MLI_{norm}) \quad (12)$$

The weighting factors in the Balanced Score were selected to reflect a performance-oriented calibration objective, prioritizing engine efficiency and output, while mechanical loading serves as a limiting constraint. A weight of 0.6 was assigned to the performance score, while a weight of 0.4 was assigned to the loading term.

4.5. Operating envelope construction

An operating envelope was constructed in a two-dimensional pressure space using peak cylinder pressure (p_{max}) and maximum pressure rise rate $(dp/d\theta)_{max}$. The injection timing sweep was mapped to identify transitions between moderate and high-intensity combustion regimes. The envelope was used to identify operating regions characterized by rapid increases in pressure gradients.

5. Results and discussion

Simulations were performed using the engine specifications (Appendix, Table 1) and operating conditions (Appendix, Table 2). Calibrated Diesel-RK outputs were used to extract performance, combustion, pressure development and gas force parameters. Raw and post-processed data are provided in Appendix Tables A3 and A4. The main analysis focuses on 2000 rpm for all loads with injection timing varied from 0°CA to 20°CA, while the remaining speed cases are presented in the Appendix.

5.1. Effect of injection timing on combustion structure evolution

At 2000 rpm, CA50 showed a greater response to injection-timing variation under low-load operation than under high-load conditions (Fig. 1). At 25% and 50% load, CA50 changed by only about 1°CA despite injection advance. As the load increased further, the response weakened considerably, and CA50 remained almost unchanged, staying near 18.8°CA at 75% load and about 23.5°CA at full load.

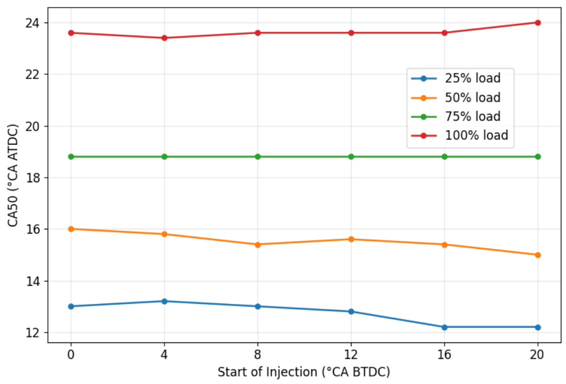

Fig. 1. Variation of combustion phasing (CA50) with injection timing at different engine loads at 2000 rpm

At low load, the longer ignition delay increases the premixing duration before ignition. Advancing the injection timing extends this period, producing a more concentrated heat-release event near top dead center and shifting the combustion centroid to earlier crank angles. With increasing load, the shorter ignition delay limits the accumulation of premixed fuel. Under these conditions, variations in injection timing no longer produce a proportional shift in the combustion centroid, leading to the observed clustering of CA50 .

Figure 2 shows that injection timing altered both combustion phasing and combustion duration. At early combustion phasing (CA50 ≈ 12–13°CA aTDC), the combustion duration remains short, indicating a concentrated heat-release event. As CA50 shifts toward 15–16°CA aTDC, combustion duration increases, indicating a transitional combustion regime. A markedly different response emerges

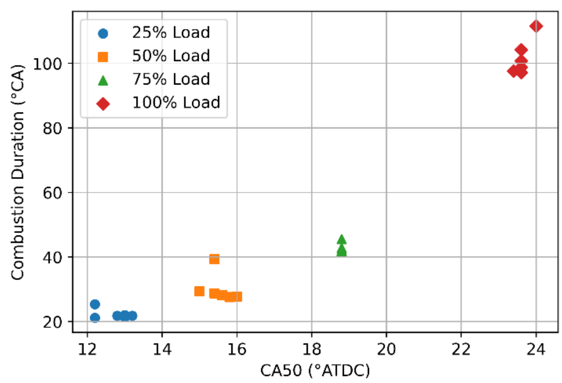

Fig. 2. Combustion structure evolution represented by the relationship between CA50 and combustion duration under injection timing variations at 2000 rpm

beyond approximately 18.8°CA aTDC, where the combustion duration increases further and eventually expands sharply at later phasing conditions.

4.2. Redistribution of combustion intensity

Figure 3 shows that the response of normalized combustion intensity to injection timing was strongly load-dependent and distinctly non-monotonic. At 25% load, it remained relatively high over the entire SOI range. At 50% load, a clear minimum appears at intermediate SOI, followed by a marked increase at more advanced timing, indicating a change in the heat-release pattern. At 75% load, the variation is smaller, with a gradual increase and a slight decline. At 100% engine load, the values remain low across all conditions. The relatively high values at low and intermediate loads indicate more temporally concentrated heat release.

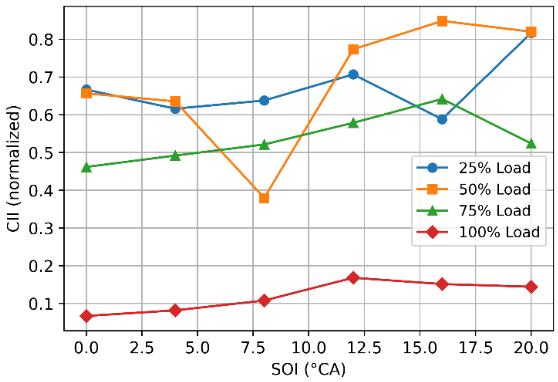

Fig. 3. Variation of normalized combustion intensity index (CII) with injection timing at 2000 rpm for different engine loads

Increasing load raised HRR_{max}, but also extended combustion duration through a stronger diffusion-controlled phase. At high load, the extended combustion duration reduced CII_{norm} despite the higher fuel quantity. Non-monotonic behaviour appeared mainly at low and intermediate loads because injection timing affected heat-release development differently across load conditions. At certain SOI values, advancing injection increased premixed combustion intensity, whereas at others it broadened the heat-release process and increased combustion duration.

Figure 4 summarizes the maximum attainable combustion intensity across the speed–load domain together with the corresponding optimal injection timing. At low load, high normalized CII values approaching unity were obtained, particularly at 1000–1500 rpm, whereas at high load the achievable intensity remained substantially lower, with values typically below 0.3 at low and intermediate speeds and reaching only about 0.4 at higher speeds.

At low load, the combustion event remained temporally compact, allowing a large fraction of the energy to be released within a narrow crank-angle interval. At high load, the extended diffusion-controlled phase broadened the combustion interval and reduced temporal concentration despite the higher energy release.

The optimal combustion structure varied across the investigated operating conditions. At lower speeds, higher CII values were sustained due to a longer available time for rapid energy release, whereas higher speeds reduced the achievable concentration, particularly when combined with high load.

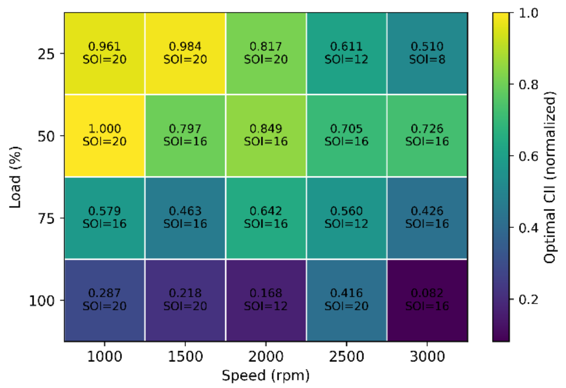

Fig. 4. Speed–load map of combustion intensity redistribution at the optimal injection timing condition

The corresponding optimal injection timing values, indicated in Fig. 4, vary systematically across the operating domain. At low load (25%), the optimal timing is predominantly advanced (SOI ≈ 20°CA) at low and intermediate speeds, shifting toward more retarded values (SOI ≈ 12–8°CA) at higher speeds. At medium load (50%), the optimal timing stabilizes around SOI ≈ 16°CA across most speeds. A similar trend is observed at 75% load, where SOI ≈ 16°CA remains dominant, with slight shifts toward 12°CA at higher speeds. At full load (100%), the optimal timing spans a broader range (SOI ≈ 12–20°CA), reflecting the increased sensitivity of combustion structure to operating conditions. Accordingly, the map illustrates how combustion characteristics varied across the speed–load domain under different injection timing conditions.

5.3. Injection timing – induced pressure evolution

5.3.1. Evolution of maximum cylinder pressure

Following the redistribution of combustion intensity described in Section 4.2, the resulting response of in-cylinder pressure development was evaluated under different injection timing conditions. The analysis considers peak cylinder pressure and pressure rise rate as the main indicators of pressure-driven engine response.

The variation of maximum cylinder pressure with injection timing at 2000 rpm exhibits a monotonic increase with injection advance. This response became more pronounced at higher loads as heat release shifted toward higher-pressure conditions. As shown in Fig. 5, peak pressure increases from about 53–61 bar at retarded injection to around 82–106 bar at advanced injection, with the highest values at full load. Advancing injection timing shifted heat release toward the compression–expansion transition at higher pressure. The pressure increase across the injection timing range grew from about 25–30 bar at low load to more than 40 bar at full load. However, peak pressure reflects the overall pressure magnitude rather than the temporal distribution of heat release. Comparison with Fig. 3 shows that while CII varied strongly with load and injection timing, peak pressure increased more uniformly with injection advance. Although peak pressure increased monotonically with injection advance, it did not fully reflect the variation in heat-release intensity and pressure-rise response.

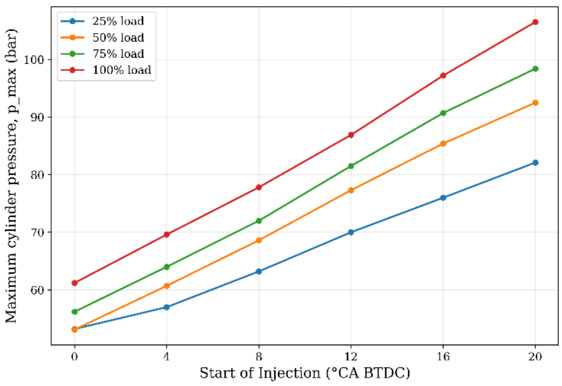

Fig. 5. Variation of maximum cylinder pressure with injection timing at different engine loads (2000 rpm)

5.3.2. Development of maximum pressure rise rate

The variation in the maximum pressure rise rate with injection timing at 2000 rpm showed a strong, load-dependent, nonlinear response. As shown in Fig. 6, $(dp/d\theta)_{max}$ increased from approximately 1.2–1.5 bar/°CA under retarded injection conditions to about 3.4–5.5 bar/°CA at advanced injection timing, with the highest values observed at high load. Earlier injection extended the premixed fuel–air preparation period before ignition, increasing the fraction of rapidly released energy near the start of combustion. Consequently, relatively small phasing shifts produced disproportionately large increases in pressure-rise rate, particularly under high-load operation, where the larger fuel quantity intensified premixed combustion. Comparison with Fig. 3 indicates that the pressure-rise response followed combustion-intensity redistribution more closely than peak cylinder pressure. Accordingly, the pressure-rise response provided clearer differentiation of loading severity than peak pressure alone.

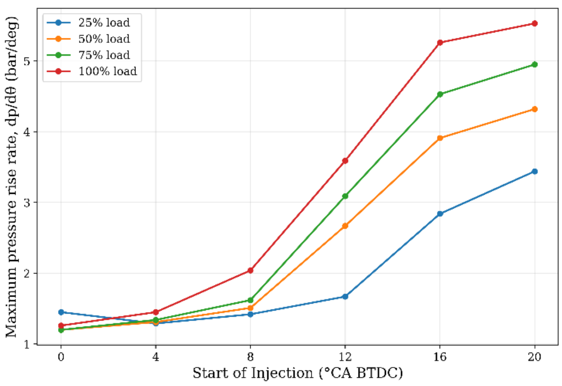

Fig. 6. Effect of injection timing on maximum pressure rise rate at different engine loads (2000 rpm)

5.4. Combustion intensity–mechanical loading coupling

5.4.1. Combustion intensity influence on pressure development

The following analysis examines the relationships among combustion intensity, pressure development, and mechanical loading as injection timing varies. Mechanical loading was evaluated using peak pressure, pressure-rise rate, and the mechanical loading index (MLI).

Figure 7 shows that the relationship between normalized combustion intensity and maximum pressure rise rate remained strongly dependent on engine load across the investigated operating conditions. At 25% and 50% load, relatively high CII_{norm} values were generally associated with higher pressure rise rates, whereas at 75% and especially 100% load, the pressure rise rate continued to increase, even though CII_{norm} remained moderate or very low. For example, at 100% load, CII_{norm} remained below about 0.17, while the maximum pressure rise rate exceeded 5 bar/°CA.

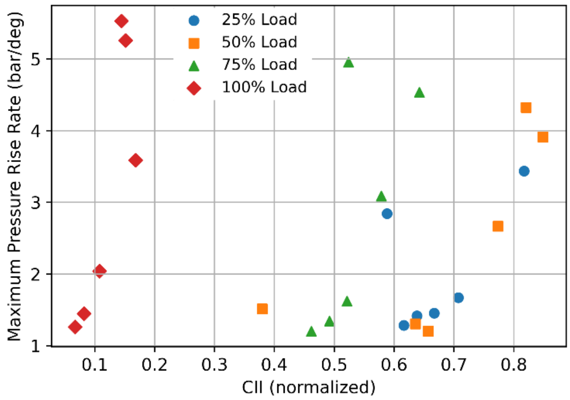

Fig. 7. Relationship between combustion intensity index and maximum pressure rise rate at different engine loads (2000 rpm)

At low and intermediate loads, a higher CII_{norm} reflects a more compact heat-release event, in which a relatively large fraction of the released energy is concentrated within a short crank-angle interval. Accordingly, low- and medium-load conditions showed higher pressure-rise response with increasing CII_{norm}.

At higher loads, the combustion characteristics change. The duration of combustion becomes longer, and the diffusion-controlled phase becomes more pronounced, which lowers CII_{norm} by reducing the temporal concentration of heat release. At the same time, the larger fuel quantity and stronger overall heat release increase the absolute pressure response, so the maximum pressure rise rate continues to increase even when the normalized combustion intensity remains low.

Accordingly, similar combustion intensities produced different pressure-rise responses across load conditions because both the heat-release concentration and the total released energy influenced pressure development. As a result, the 100% load cases occupied the low-CII_{norm}, high-$(dp/d\theta)_{max}$ region, whereas lower-load conditions remained associated with higher CII_{norm} values at comparatively lower pressure-rise rates. These results indicate that the relationship between combustion intensity and pressure-rise response depended strongly on operating conditions.

5.4.2. Pressure rise–driven mechanical loading response

Figure 8 shows the variation of maximum gas force with the maximum pressure-rise rate under the investigated operating conditions. Gas force increased from approximately 50–70 kN at low pressure-rise rates (~1–2 bar/°CA) to values exceeding 100 kN as $(dp/d\theta)_{max}$ approached 5 bar/°CA.

Despite the overall increase, the relationship remained load-dependent. Similar pressure-rise rates produced different gas-force levels across the investigated loads. High-load operation occupied the upper gas-force region because larger fuel quantities generated higher absolute cylinder pressure even under comparable pressure-rise conditions.

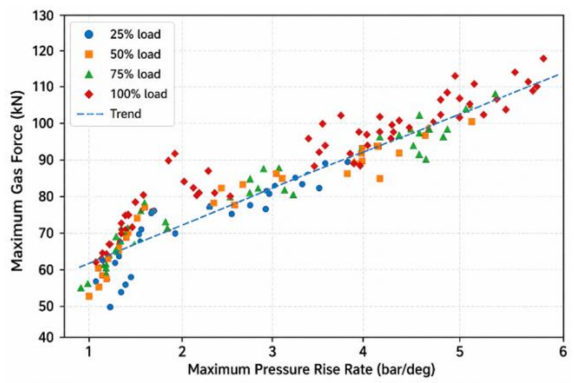

Fig. 8. Relationship between maximum pressure-rise rate and maximum gas force under different operating conditions

The spread of operating points reflects variations in combustion phasing and pressure development. The results also show that the pressure-rise rate alone could not fully represent mechanical loading severity, since gas-force generation depended on both the pressure-rise response and the absolute pressure level. This combined effect is incorporated later through the mechanical loading index (MLI).

5.4.3. Mechanical loading index response

Figure 9 shows that MLI_{norm} increased with injection advance across all loads, with a stronger response at high loads. At 25% load, MLI_{norm} varied within a limited range (≈0.04–0.40), whereas at full load it increased to approximately 0.93, indicating a stronger mechanical loading response at high load.

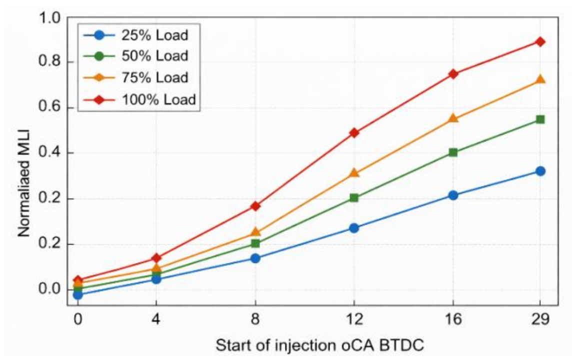

Fig. 9. Mechanical loading index variation with injection timing at different engine loads (2000 rpm)

At high load, identical injection-timing shifts produced larger increases in MLI_{norm} because of the combined effect of pressure-rise response and energy release. Combustion phasing influenced pressure development, whereas load controlled the magnitude of the pressure response. Higher fuel energy intensified pressure development and accelerated the increase in mechanical loading at high load.

4.5. Trade-off between performance and mechanical loading

Figure 10 shows the trade-off between performance and mechanical loading at 2000 rpm for different load conditions. Higher performance was accompanied by increased mechanical loading. Operating points with moderate performance (∼0.45) corresponded to low loading levels ($\lesssim$ 0.1), whereas high-performance conditions (∼0.7) were associated with substantially higher loading ($\gtrsim$ 0.7). At 25% load, operation remained within a low-loading region with limited performance gains, whereas at 100% load, both performance and loading increased substantially.

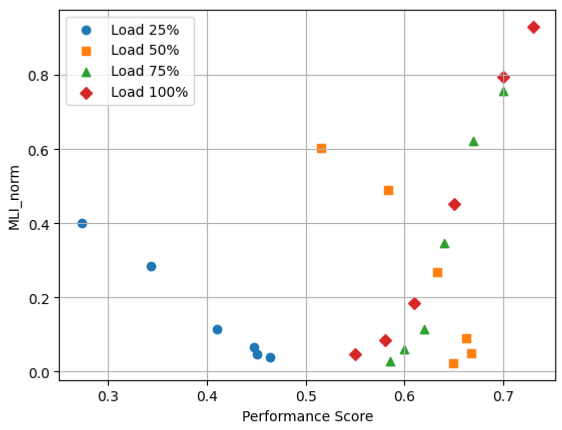

Fig. 10. Performance–mechanical loading trade-off map at 2000 rpm under different engine load conditions

Higher performance was associated with stronger pressure development and increases in both p_{max} and $(dp/d\theta)_{max}$, which amplified mechanical loading. Advanced injection produced stronger pressure development at high load.

At 25% load, the lower fuel quantity limited pressure development. At 50–75% load, sensitivity to injection timing increased as premixed combustion became more pronounced. At 100% load, the response became steeper because of the simultaneous increase in p_{max} and $(dp/d\theta)_{max}$. Higher CII values were associated with more concentrated heat release and steeper pressure gradients, whereas at high load, the increase in loading became increasingly influenced by energy release.

4.6. Optimal injection timing envelope

Two optimality criteria were considered in this study: a combustion-based optimum derived from CII and a performance-loading optimum based on the Balanced Score. The optimal injection timing varied with engine speed and load. Figure 4 represents combustion-based optima, whereas the present section considers combined performance and loading conditions.

Figure 11 shows the optimal injection timing at 2000 rpm based on the Balanced Score, which combines performance and mechanical loading. The optimal operating conditions were identified using the Balanced Score ranking. The data formed distinct load-dependent trajectories across the investigated conditions. The Balanced Score response varied with load and injection timing.

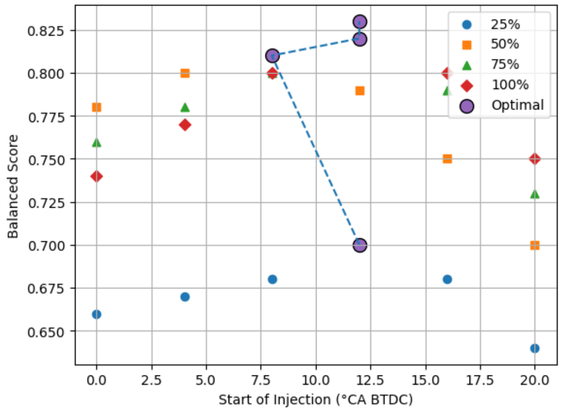

Fig. 11. Optimal injection timing envelope at 2000 rpm

At low load (25%), the response to injection timing remains limited, reflecting insufficient energy release to generate strong pressure development, and thus only marginal variation in the Balanced Score. In contrast, at intermediate loads (50–75%), a well-defined optimal region emerges around SOI ≈ 8–12°CA bTDC, where the balance between performance and mechanical loading was most favorable. At full load (100%), the trend shifts: excessive injection advancement leads to a deterioration in the Balanced Score, despite high performance levels, due to rapid mechanical loading.

This response arises from the coupling between combustion structure and pressure development. Advancing the injection increased combustion intensity and the pressure-rise rate, thereby increasing mechanical loading. At high load, larger fuel quantities increased the pressure response even under less concentrated combustion conditions. Similar p_{max} values were associated with different pressure-rise responses under different load conditions. The optimal points shifted with load due to the combined effects of combustion phasing and energy release.

These results indicate that performance improvement must be considered together with mechanical loading during engine calibration. The optimal injection timing identified in Fig. 11 differed from the combustion-based optimum shown in Fig. 4 because the Balanced Score included both performance and mechanical loading. Combustion-optimal conditions did not always correspond to the lowest mechanical loading conditions.

5.7. Physical interpretation of phasing-driven loading mechanism

The preceding results show that mechanical loading was influenced by changes in combustion intensity and pressure-rise response under injection timing variations. Advancing injection timing increased combustion intensity (CII) and pressure-rise rate, $(dp/d\theta)_{max}$. Similar peak-pressure levels were associated with different pressure-rise responses and mechanical loading responses.

Injection timing controls structural loading by influencing combustion-zone evolution. Moderate injection advance improved combustion phasing and engine performance. Further injection advance increased $(dp/d\theta)_{max}$ more rapidly than performance improvement, leading to higher mechanical loading.

6. Conclusions

The present study investigated the relationships among combustion characteristics, pressure development, and mechanical loading in a turbocharged diesel engine under injection timing variations. The results showed that combustion-optimal injection timing did not always correspond to the lowest mechanical loading conditions, indicating that injection timing selection depends strongly on operating condition and loading response. Mechanical loading was more strongly influenced by pressure-rise response than by peak pressure alone, particularly under advanced injection and high-load conditions. The main conclusions are summarized as follows:

1. Injection timing modified combustion phasing and changed the distribution of heat release during the engine cycle. Advancing the injection moved the main combustion phase toward earlier crank angles and increased the temporal concentration of heat release.
2. Combustion intensity strongly influenced pressure development, where the maximum pressure rise rate increased from approximately 1.2–1.5 bar/°CA under retarded injection to values exceeding 5 bar/°CA at advanced injection and high load.
3. The maximum gas force exceeded 100 kN under full-load operation. The results further showed that pressure-rise response provided a more representative indication of combustion-driven loading severity than peak pressure alone.
4. The mechanical loading index (MLI) increased with injection advance across the investigated conditions. Advanced injection improved engine performance but simultaneously increased pressure-induced mechanical loading.
5. The optimal injection timing therefore, varied with load and operating condition. Moderate injection advance produced near-maximum performance while maintaining lower mechanical loading than highly advanced injection conditions.

The CII and MLI indicators enabled comparison of combustion characteristics and mechanical loading across operating conditions.

Nomenclature

aHRR	apparent heat release rate, J/°CA
BP	brake power, kW
BSFC	brake specific fuel consumption, kg/kWh
BTE	brake thermal efficiency,
CA05	crank angle at 5% heat release, °CA
CA50	crank angle at 50% cumulative heat release, °CA
CA95	crank angle at 95% heat release, °CA
CII	combustion intensity index, –
CII_{norm}	normalized combustion intensity index, –
$dQ/d\theta$	heat release rate per crank angle, J/°CA
EOC	end of combustion, °CA
F_{max}	maximum piston gas force, kN

HRR	heat release rate, J/°CA
HRR_{max}	maximum heat release rate, J/°CA
IMEP	indicated mean effective pressure, bar
Load (L)	engine load, %
MLI	mechanical loading index, –
MLI_{norm}	normalized mechanical loading index, –
N	engine speed, rpm
$p(\theta)$	instantaneous in-cylinder pressure, bar
p_{max}	maximum in-cylinder pressure, bar
$Perf_{Score}$	performance score, –
PR	turbocharger pressure ratio, –
Q	heat release, J
SOI	start of injection, °CA bTDC
TDC	top dead center, –
$(dp/d\theta)_{max}$	maximum pressure rise rate, bar/°CA

Bibliography

[1] Ashok B, Nanthagopal K. Eco friendly biofuels for CI engine applications. Elsevier eBooks. 2019:407-440. https://doi.org/10.1016/b978-0-08-102728-8.00015-2

[2] Moretto G, Hänggi S, Onder C. Optimal combustion calibration for direct-injection compression-ignition engines using multiple injections. Int J Engine Res. 2022;24(4):1414-1431. https://doi.org/10.1177/14680874221087969

[3] Luong MB, Sankaran R, Yu GH, Chung SH, Yoo CS. On the effect of injection timing on the ignition of lean PRF/air/EGR mixtures under direct dual fuel stratification conditions. Combust Flame. 2017;183:309-321. https://doi.org/10.1016/j.combustflame.2017.05.023

[4] Catalani I, Bosi L, Baroni A, Romani L, Vichi G, Bellissima A et al. In-cylinder pressure estimation in a multi-cylinder engine by combining instantaneous crankshaft speed data and a 0D thermodynamic model: numerical validation. J Phys Conf Ser. 2022;2385(1):012069. https://doi.org/10.1088/17426596/2385/1/012069

[5] Tsitsilonis K, Theotokatos G. A novel method for in-cylinder pressure prediction using engine instantaneous crankshaft torque. Proc Inst Mech Eng Part M J Eng Marit Environ. 2021;236(1):131-149. https://doi.org/10.1177/14750902211028419

[6] Ferrari A, Vassallo A. Impact of the common rail fuel injection system on performance and emissions of modern and future compression ignition engines. Energies. 2025;18(19): 5259. https://doi.org/10.3390/en18195259

[7] Belgiorno G, Dimitrakopoulos N, Di Blasio G, Beatrice C, Tunestål P, Tunér M. Effect of engine calibration parameters on gasoline partially premixed combustion performance and emissions compared to conventional diesel combustion in a light-duty Euro 6 engine. Appl Energy. 2018;228:2221-2234. https://doi.org/10.1016/j.apenergy.2018.07.098

[8] Sharma P, Chhillar A, Said Z, Huang Z, Nguyen VN, Nguyen PQP et al. Experimental investigations on efficiency and instability of combustion process in a diesel engine fueled with ternary blends of hydrogen peroxide additive/biodiesel/diesel. Energy Sources A Recover Util Environ Eff. 2022;44(3):5929-5950. https://doi.org/10.1080/15567036.2022.2091692

[9] Sadabadi KK, Shahbakhti M, Bharath AN, Reitz RD. Modeling of combustion phasing of a reactivity-controlled compression ignition engine for control applications. Int J Engine Res. 2015;17(4):421-435. https://doi.org/10.1177/1468087415583773

[10] Zheng Z, Lappas P, Shamekhi A, Wang X, Mikulski M. Advancements in detecting combustion events through vibration analysis in internal combustion engines: a literature review. Mech Syst Signal Process. 2025;241:113539. https://doi.org/10.1016/j.ymssp.2025.113539

[11] Lou D, Song G, Zhang Y, Fang L, Deng Y. Experimental study on the effects of injection pressure and injection timing on combustion and emissions in a direct-injection hydrogen engine. Case Stud Therm Eng. 2025;75:107235. https://doi.org/10.1016/j.csite.2025.107235

[12] Ezhumalai M, Govindasamy M. Optimization of ignition delay and combustion efficiency in diesel-biodiesel-ethanol blends for compression ignition engine. Case Stud Therm Eng. 2025;68:105823. https://doi.org/10.1016/j.csite.2025.105823

[13] Baek HM, Lee HM. Experimental investigation of ringing intensity and combustion noise level from biodiesel fuel in CRDI diesel engine with various injection timings. J Adv Mar Eng Technol. 2022;46(2):56-63. https://doi.org/10.5916/jamet.2022.46.2.56

[14] ADhahad H, Abdulhadi MA, MAlfayydh E, Megaritis T. Influence of injection pressure on combustion and emission characteristics of a common-rail HSDI diesel engine. Thi-Qar Univ J Eng Sci. 2014;5(1):55-72. https://doi.org/10.31663/utjes.v5i1.597

[15] Zhang P, Ni J, Shi X, Yin S, Zhang D. Effects of ignition timing on combustion characteristics of a gasoline direct injection engine with added compressed natural gas under partial load conditions. Processes. 2021;9(5):755. https://doi.org/10.3390/pr9050755

[16] Liang X, Yang G, Dai P, Lin X, Zhang X, Li L. Experimental investigation on the relationship between in-cylinder pressure rise rate and combustion noise of a diesel engine. Appl Acoust. 2024;223:110084. https://doi.org/10.1016/j.apacoust.2024.110084

[17] Pham VC, Le VV, Choi J, Lee W. CFD analysis of equivalence ratio effects on combustion and emissions in a methanol–diesel dual-fuel marine engine. Energies. 2026;19(3): 626. https://doi.org/10.3390/en19030626

[18] Marriott CD, Reitz RD. Experimental investigation of direct-injection gasoline for premixed compression ignited combustion phasing control. SAE Technical Paper 2002-01-0418. 2002. https://doi.org/10.4271/2002-01-0418

[19] Kawakami T, Liu J. Enhancing combustion characteristics in a constant volume chamber using a novel multi-injection system for liquid fuel and propane-air stratified mixtures. Combust Engines. 2025;204(1):27-34. https://doi.org/10.19206/ce-208773

[20] Kneba Z, Stepanenko D, Rudnicki J. Numerical methodology for evaluation the combustion and emissions characteristics on WLTP in the light duty dual-fuel diesel vehicle. Combust Engines. 2021;189(2):94–102. https://doi.org/10.19206/ce-143334

[21] Siadkowska K, Barański G. Combustion stability for early and late direct hydrogen injection in a dual fuel diesel engine. Combust Engines. 2023;196(1):89-98. https://doi.org/10.19206/ce-171390

Eihab A. Raouf, DEng. – Department of Mechanical Engineering, College of Engineering, Qassim University, Buraydah 51452, Saudi Arabia.

e-mail: *eomer@qu.edu.sa*

Appendix

Table A1. Specifications of the investigated engine and applied numerical settings

Engine type	4HK1 – 5.2L Turbo Diesel	EVO / EVC	48°CA bBDC / 14°CA aTDC
No. of cylinder	4-cylinder, In-line	Connecting rod length	220 mm
Valve mechanism	16-valve, chain drive	Injection timing (SOI)	20°CA bTDC (baseline setting)
Combustion Chamber	Bowl-in-piston	Injection duration (equivalent crank angle, based on 4 ms)	At 1000 rpm → 24 °CA
Fuel system	Direct injection (common rail)		At 2000 rpm → 48 °CA
Displacement	5193 cm^3		At 3000 rpm → 72 °CA
Bore × Stroke	115 mm × 125 mm		At 4000 rpm → 96 °CA
Compression ratio	16.5: 1	Nozzle hole diameter	≈ 0.18 mm
Max output power	136 kW at 2600 rpm	Spray cone angle	150°
Max torque	480 N · m at 1600 rpm	Number of nozzle holes	7
IVO / IVC	19°CA bTDC / 53°CA aBDC	Ambient parameters	P_0 = 1 bar, T_0 = 313 K

Table A2. Load definition and corresponding fuel injection quantities at various engine speeds

Engine speed [rpm]	Load [%]	Target torque [N · m]	Fuel mass per cycle [g/cycle]
1000	25	107.8	0.0295
	50	215.5	0.0497
	75	335.3	0.0700
	100	437.5	0.1200
1500	25	135.8	0.0307
	50	242.5	0.0498
	75	358.3	0.0735
	100	475.2	0.1100
1600 (Reference)	25	120.5	0.0245
	50	241.0	0.0457
	75	361.5	0.0730
	100	482.0	0.1059
2000	25	122.3	0.0296
	50	241.5	0.0508
	75	361.8	0.0727
	100	478.0	0.1033
2500	25	116.2	0.0307
	50	242.0	0.0520
	75	350.2	0.0730
	100	470.9	0.1000
3000	25	091.1	0.0282
	50	245.0	0.0547
	75	346.7	0.0768
	100	462.3	0.1100

Table A3. Raw performance, combustion phasing, and pressure-trace indicators for the SOI sweep matrix (1000–3000 rpm; 25–100% load)

Case n_Load_SOI	BP	BTE	BSFC	Ignition delay	CA5	CA50	CA95	pmax	Apmax	dp/dθ	HRR_{max}
rpm_%_°CA bTDC	kW	–	kg/kWh	°CA	°CA aTDC	°CA aTDC	°CA aTDC	bar	°CA aTDC	bar/°CA	J/°CA
1000rpm_25%_SOI=0	13.0	0.312	0.2716	4.1	2	12.4	24	51.4	0	1.41	67.30
1000rpm_25%_SOI=4	13.2	0.315	0.2689	4.0	1.8	12.4	23.8	57.2	8	1.30	65.30
1000rpm_25%_SOI=8	13.0	0.311	0.2722	4.1	1.8	12	23.2	64.5	8	1.45	66.00
1000rpm_25%_SOI=12	12.6	0.302	0.2803	4.7	1.8	11.4	22.2	72.2	7	2.36	73.60
1000rpm_25%_SOI=16	12.0	0.287	0.2954	5.9	2.8	11.2	22.4	78.9	5	3.22	79.30
1000rpm_25%_SOI=20	11.3	0.271	0.3123	7.7	3.6	10.8	24.8	83.4	3	3.82	90.70
1000rpm_50%_SOI=0	25.1	0.357	0.2373	3.9	2.2	14.6	29.8	53.7	11	1.19	76.50
1000rpm_50%_SOI=4	25.5	0.362	0.2342	3.7	2.2	14.6	29.6	62.1	11	1.31	92.00
1000rpm_50%_SOI=8	25.4	0.361	0.2349	3.8	2	14.4	29.4	71.3	9	1.59	90.40
1000rpm_50%_SOI=12	24.8	0.353	0.2402	4.3	2	13.8	29	80.6	8	3.05	89.90
1000rpm_50%_SOI=16	23.9	0.340	0.2495	5.4	2.6	13.6	29	89.3	6	4.08	113.89
1000rpm_50%_SOI=20	22.7	0.322	0.2627	7.1	3.6	13.2	32.4	96.3	4	4.71	126.90
1000rpm_75%_SOI=0	34.6	0.349	0.2425	4.1	2.2	18	53.4	50.5	11	1.01	106.00
1000rpm_75%_SOI=4	35.5	0.358	0.2365	3.9	2.2	17.8	51.4	58.2	10	1.19	103.50
1000rpm_75%_SOI=8	35.2	0.355	0.2389	4.1	2.2	17.6	62.2	66.6	10	1.87	112.40
1000rpm_75%_SOI=12	35.5	0.358	0.2368	5.0	2	17	50.4	75.1	9	3.22	130.60
1000rpm_75%_SOI=16	34.7	0.350	0.2422	6.3	3.4	17.6	51	83.5	7	4.59	143.90
1000rpm_75%_SOI=20	33.3	0.336	0.2519	8.1	4.2	17.6	57.2	90.2	5	4.74	146.90

Table A3. cont

Case n_Load_SOI	BP	BTE	BSFC	Ignition delay	CA5	CA50	CA95	pmax	Apmax	dp/dθ	HRR_{max}
rpm_%_°CA bTDC	kW	–	kg/kWh	°CA	°CA aTDC	°CA aTDC	°CA aTDC	bar	°CA aTDC	bar/°CA	J/°CA
1000rpm_100%_SOI=0	44.0	0.259	0.3273	2.8	3	23.6	119	57.0	11	1.17	130.60
1000rpm_100%_SOI=4	45.2	0.266	0.3189	2.8	3	23.6	117.8	65.5	9	1.37	129.10
1000rpm_100%_SOI=8	45.8	0.270	0.3143	3.0	2.8	23.4	115.4	74.0	8	2.21	127.90
1000rpm_100%_SOI=12	45.9	0.270	0.3136	3.4	2.4	22.8	111.8	83.0	7	3.91	142.90
1000rpm_100%_SOI=16	45.3	0.267	0.3177	4.4	2.2	22	107.8	92.0	7	4.45	176.20
1000rpm_100%_SOI=20	44.0	0.259	0.3273	5.7	3.4	22.4	107.6	100.5	6	4.93	215.50
1500rpm_25%_SOI=0	20.7	0.317	0.2674	6.5	3.2	12.4	24.2	45.7	0	1.25	77.40
1500rpm_25%_SOI=4	21.2	0.325	0.2608	5.8	2.8	12.4	24.4	51.8	8	1.12	74.00
1500rpm _25%_SOI=8	21.3	0.327	0.2589	6.0	2.8	12.4	24.4	58.3	8	1.27	76.20
1500rpm _25%_SOI=12	21.1	0.323	0.2619	7.0	3.4	12.2	24.6	65.0	7	1.93	82.40
1500rpm _25%_SOI=16	20.7	0.317	0.2669	8.7	4	11.6	27	71.0	6	2.92	84.40
1500rpm _25%_SOI=20	20.2	0.309	0.2738	11.3	4	12	23.8	76.6	5	3.48	86.20
1500rpm _50%_SOI=0	36.8	0.348	0.2434	4.6	2	15	31.6	49.0	11	1.05	90.50
1500rpm _50%_SOI=4	37.7	0.357	0.2376	4.6	2	15.2	31.6	55.9	9	1.17	91.40
1500rpm _50%_SOI=8	38.1	0.360	0.2354	4.9	2	14.8	31.8	63.6	9	1.41	96.30
1500rpm _50%_SOI=12	37.9	0.358	0.2365	5.8	3	15.2	33	71.6	8	2.60	108.60
1500rpm _50%_SOI=16	37.3	0.352	0.2405	7.4	3.8	15	34.4	79.0	7	4.10	114.40
1500rpm _50%_SOI=20	36.4	0.344	0.2463	9.6	4.4	14.2	36	85.9	5	4.29	113.50
1500rpm _75%_SOI=0	53.9	0.345	0.2452	3.9	2.4	19.2	53.4	51.6	11	1.07	105.30
1500rpm _75%_SOI=4	55.4	0.355	0.2387	4.0	2.4	19.2	54.2	59.1	9	1.22	107.80
1500rpm _75%_SOI=8	56.4	0.361	0.2348	4.2	2.2	19.2	54.2	67.4	10	1.84	115.30
1500rpm _75%_SOI=12	56.5	0.362	0.2340	4.9	2.2	18.6	54.4	76.0	9	3.13	126.40
1500rpm _75%_SOI=16	56.0	0.358	0.2363	6.3	3.4	19	56.4	84.5	7	4.50	140.10
1500rpm _75%_SOI=20	54.8	0.351	0.2414	8.1	4.2	19.2	59.4	91.7	6	4.57	142.30
1500rpm _100%_SOI=0	70.8	0.303	0.2797	3.8	2.6	23	110	59.4	11	1.21	129.70
1500rpm _100%_SOI=4	73.2	0.313	0.2705	3.7	2.6	23.2	108.2	67.6	9	1.40	129.80
1500rpm _100%_SOI=8	74.7	0.319	0.2652	4.0	2.6	23	108.2	76.0	8	2.14	137.90
1500rpm_100%_SOI=12	75.2	0.322	0.2631	4.4	2.2	22.6	107.8	85.4	8	3.83	153.40
1500rpm_100%_SOI=16	72.8	0.312	0.2718	5.5	3	22.8	136.8	95.0	8	4.98	179.20
1500rpm_100%_SOI=20	73.4	0.314	0.2699	7.2	4	22.8	113.2	104.2	6	5.61	200.80
2000rpm_25%_SOI=0	24.4	0.290	0.2917	6.7	3.4	13	24.8	53.2	0	1.45	70.90
2000rpm_25%_SOI=4	25.2	0.301	0.2817	6.1	3	13.2	24.8	57.0	8	1.29	68.60
2000rpm_25%_SOI=8	25.6	0.305	0.2773	6.3	3.2	13	25.2	63.2	6	1.42	70.80
2000rpm_25%_SOI=12	25.6	0.306	0.2772	7.1	3.6	12.8	25.4	70.0	6	1.67	75.10
2000rpm_25%_SOI=16	25.3	0.302	0.2805	8.7	4.2	12.2	29.6	76.0	5	2.84	77.60
2000rpm_25%_SOI=20	24.9	0.297	0.2850	11.2	3.8	12.2	25	82.1	5	3.44	80.70
2000rpm_50%_SOI=0	49.1	0.341	0.2483	4.6	2.4	16	30.2	53.1	10	1.20	91.20
2000rpm_50%_SOI=4	50.6	0.352	0.2409	4.6	2.2	15.8	29.8	60.7	8	1.31	88.60
2000rpm_50%_SOI=8	50.6	0.352	0.2409	4.9	2.2	15.4	41.6	68.6	9	1.51	93.40
2000rpm_50%_SOI=12	51.6	0.359	0.2362	5.4	2.8	15.6	31	77.3	8	2.67	103.30
2000rpm_50%_SOI=16	51.0	0.355	0.2389	6.7	3.4	15.4	32.2	85.4	7	3.91	112.60
2000rpm_50%_SOI=20	50.0	0.348	0.2437	8.7	4.4	15	33.8	92.5	6	4.32	112.20
2000rpm_75%_SOI=0	71.5	0.347	0.2441	4.5	2.4	18.8	45.2	56.2	10	1.20	113.00
2000rpm_75%_SOI=4	74.1	0.360	0.2354	4.5	2.4	18.8	44.2	64.0	8	1.34	114.50
2000rpm_75%_SOI=8	75.7	0.368	0.2305	4.7	2.4	18.8	44.4	72.0	9	1.62	119.10
2000rpm_75%_SOI=12	76.5	0.371	0.2282	5.2	2.8	18.8	44.8	81.5	9	3.09	127.00
2000rpm_75%_SOI=16	76.2	0.370	0.2289	6.5	3.6	18.8	46.4	90.7	7	4.53	138.30
2000rpm_75%_SOI=20	75.1	0.364	0.2325	8.5	4.2	18.8	49.8	98.4	6	4.95	129.70
2000rpm_100%_SOI=0	93.7	0.320	0.2647	4.3	2.6	23.6	99.8	61.2	11	1.26	130.70
2000rpm_100%_SOI=4	97.4	0.333	0.2544	4.3	2.6	23.4	100.2	69.6	8	1.45	136.00
2000rpm_100%_SOI=8	100.2	0.342	0.2474	4.5	2.6	23.6	101.4	77.8	7	2.04	146.10
2000rpm_100%_SOI=12	101.9	0.348	0.2433	5.0	2.8	23.6	103.6	86.9	8	3.59	169.00
2000rpm_100%_SOI=16	102.2	0.349	0.2427	6.1	3.4	23.6	107.6	97.2	7	5.26	169.00
2000rpm_100%_SOI=20	101.0	0.345	0.2456	7.8	4.2	24	115.8	106.5	6	5.53	178.40
2500rpm_25%_SOI=0	28.5	0.262	0.3230	5.7	3	14	26.2	49.5	0	1.35	64.40
2500rpm_25%_SOI=4	29.7	0.273	0.3101	5.7	3	14.2	26.4	53.3	8	1.21	64.50
2500rpm _25%_SOI=8	30.4	0.280	0.3029	6.0	3.2	14	26.4	59.3	7	1.33	67.90
2500rpm _25%_SOI=12	30.7	0.283	0.2997	6.8	3.6	13.8	26.8	65.8	7	1.57	72.60
2500rpm _25%_SOI=16	30.7	0.282	0.3003	8.5	4.2	13	32.2	71.7	5	2.74	75.40
2500rpm _25%_SOI=20	30.4	0.279	0.3033	11.0	4	12.8	28.6	77.5	5	3.29	77.00
2500rpm _50%_SOI=0	59.6	0.324	0.2616	5.2	2.8	16.8	32.8	50.7	11	1.14	91.40
2500rpm _50%_SOI=4	62.0	0.337	0.2515	5.1	2.8	17	32.2	57.7	8	1.23	91.90

Table A3. cont

Case n_Load_SOI	BP	BTE	BSFC	Ignition delay	CA5	CA50	CA95	pmax	Apmax	dp/dθ	HRR_{max}
rpm_%_°CA bTDC	kW	–	kg/kWh	°CA	°CA aTDC	°CA aTDC	°CA aTDC	bar	°CA aTDC	bar/°CA	J/°CA
2500rpm _50%_SOI=8	63.5	0.345	0.2458	5.4	3	17	32.6	64.6	8	1.43	97.10
2500rpm _50%_SOI=12	64.1	0.348	0.2435	6.1	3.4	17	33.6	72.5	8	2.39	103.30
2500rpm _50%_SOI=16	63.9	0.347	0.2442	7.6	4.2	16.8	35.4	80.3	7	3.76	107.30
2500rpm _50%_SOI=20	62.6	0.340	0.2491	9.9	4.4	16	44.4	86.7	5	3.98	105.30
2500rpm _75%_SOI=0	85.6	0.331	0.2559	4.8	2.6	19.4	45.2	57.0	10	1.24	111.90
2500rpm _75%_SOI=4	89.1	0.345	0.2459	4.8	2.6	19.6	44.8	64.5	8	1.37	112.20
2500rpm _75%_SOI=8	91.7	0.355	0.2389	5.0	2.8	19.8	44.6	72.3	8	1.62	116.70
2500rpm _75%_SOI=12	93.1	0.360	0.2353	5.6	3.2	19.8	45.4	81.2	8	2.90	125.00
2500rpm _75%_SOI=16	90.9	0.351	0.2410	6.7	3.8	19.8	62.6	90.3	7	4.29	133.20
2500rpm _75%_SOI=20	92.1	0.356	0.2378	8.7	4.4	19.8	51.4	98.0	6	4.69	134.30
2500rpm _100%_SOI=0	114.0	0.322	0.2631	4.4	2.8	23.2	67.6	65.7	10	1.44	126.00
2500rpm _100%_SOI=4	119.4	0.337	0.2513	4.4	2.8	23	65.6	74.4	8	1.58	126.30
2500rpm _100%_SOI=8	123.3	0.348	0.2434	4.6	2.6	22.8	65.6	83.1	7	1.91	134.00
2500rpm_100%_SOI=12	125.7	0.355	0.2386	5.1	3	23.2	66.6	92.3	8	3.52	142.50
2500rpm_100%_SOI=16	126.6	0.357	0.2370	5.8	3.4	23.2	68.6	103.1	7	4.78	159.50
2500rpm_100%_SOI=20	125.7	0.355	0.2388	7.5	4.2	23.4	73.2	113.2	6	5.56	171.70
3000rpm_25%_SOI=0	26.2	0.218	0.3879	5.6	3	14	26.2	50.1	0	1.37	58.80
3000rpm_25%_SOI=4	27.7	0.231	0.3659	5.6	3	14	25.2	53.0	7	1.24	59.20
3000rpm_25%_SOI=8	28.6	0.239	0.3548	5.9	3.2	13.8	25.6	58.7	6	1.34	62.70
3000rpm_25%_SOI=12	28.4	0.237	0.3581	6.6	3.6	14	34.2	64.4	6	1.53	65.20
3000rpm_25%_SOI=16	28.3	0.236	0.3582	8.3	4.2	13.6	33.8	69.8	5	2.58	68.30
3000rpm_25%_SOI=20	28.1	0.235	0.3612	10.7	4.2	13.2	30.8	74.9	5	2.96	68.60
3000rpm_50%_SOI=0	71.4	0.307	0.2757	5.1	2.6	17.2	33.2	54.0	10	1.24	94.40
3000rpm_50%_SOI=4	74.6	0.321	0.2641	5.1	2.6	17.4	33.4	61.1	7	1.33	95.10
3000rpm_50%_SOI=8	77.0	0.331	0.2558	5.3	2.8	17.4	33.2	68.0	7	1.52	98.80
3000rpm_50%_SOI=12	78.4	0.337	0.2512	5.9	3.4	17.6	34	75.9	8	2.43	102.90
3000rpm_50%_SOI=16	78.5	0.338	0.2508	7.2	4	17.6	35	84.1	7	3.90	108.70
3000rpm_50%_SOI=20	77.7	0.334	0.2534	9.2	4.6	17.2	37.6	90.9	6	4.20	106.40
3000rpm_75%_SOI=0	99.8	0.306	0.2770	4.9	2.8	21.2	54.4	55.8	10	1.23	110.90
3000rpm_75%_SOI=4	105.1	0.322	0.2630	4.9	2.6	21.4	52.4	63.2	8	1.34	110.00
3000rpm_75%_SOI=8	108.9	0.334	0.2539	5.1	3	21.6	53	70.3	7	1.58	113.60
3000rpm_75%_SOI=12	111.5	0.342	0.2480	5.7	3.4	21.8	53.6	78.4	8	2.76	122.30
3000rpm_75%_SOI=16	112.3	0.344	0.2462	7.0	4	22	56.4	87.0	7	4.45	132.20
3000rpm_75%_SOI=20	111.4	0.341	0.2483	9.0	4.6	22	61.6	94.6	6	4.45	132.20
3000rpm_100%_SOI=0	131.4	0.281	0.3013	4.7	2.8	26.2	120.8	64.2	10	1.38	135.10
3000rpm_100%_SOI=4	139.3	0.298	0.2843	4.7	2.8	26.2	114.8	72.6	8	1.54	134.10
3000rpm_100%_SOI=8	145.3	0.311	0.2725	4.9	2.8	26.2	113	80.4	6	2.30	139.40
3000rpm_100%_SOI=12	149.3	0.319	0.2652	5.4	3.2	26.6	115.6	88.8	7	3.39	149.90
3000rpm_100%_SOI=16	151.5	0.324	0.2613	6.2	3.8	27	120.2	98.6	7	5.16	162.20
3000rpm_100%_SOI=20	151.1	0.323	0.2620	7.8	4.4	27.2	129.4	108.2	6	5.32	169.50

Table A4. Calculated combustion duration, gas-force–based loading indicators (F_{max}, MLI), combustion intensity index (CII), and normalized performance metrics (BTE*, BP*, BSFC*) with the resulting Perf_Score and Balanced Score for all SOI sweep cases

Case n (rpm)_Load (%) _SOI°	Combustion duration °CA	Fmax kN	CII_{raw} J/°CA^2	CII_{norm}	MLI_{raw} bar^2/°CA	MLI_{norm}	BP*	BTE*	BSFC*	$Perf_{Score}$	Balanced score
1000rpm_25%_SOI=0	22	53.46	3.059	0.589	72.24	0.037	0.012	0.612	0.728	0.4507	0.6558
1000rpm_25%_SOI=4	22	59.47	2.968	0.562	74.21	0.040	0.013	0.632	0.745	0.4635	0.6621
1000rpm_25%_SOI=8	21.4	67.07	3.084	0.597	93.69	0.074	0.012	0.607	0.724	0.4478	0.6391
1000rpm_25%_SOI=12	20.4	75.02	3.608	0.757	170.35	0.206	0.009	0.549	0.674	0.4105	0.5637
1000rpm_25%_SOI=16	19.6	82.08	4.046	0.890	254.28	0.352	0.005	0.447	0.579	0.3436	0.4655
1000rpm_25%_SOI=20	21.2	86.74	4.278	0.961	319.00	0.464	0.000	0.346	0.474	0.2733	0.3785
1000rpm_50%_SOI=0	27.6	55.82	2.772	0.502	63.62	0.022	0.098	0.907	0.943	0.6493	0.7808
1000rpm_50%_SOI=4	27.4	64.61	3.358	0.680	81.12	0.052	0.101	0.938	0.962	0.6671	0.7794
1000rpm_50%_SOI=8	27.4	74.14	3.299	0.663	113.60	0.108	0.100	0.931	0.958	0.6630	0.7544
1000rpm_50%_SOI=12	27	83.79	3.330	0.672	246.10	0.338	0.096	0.879	0.925	0.6335	0.6451
1000rpm_50%_SOI=16	26.4	92.86	4.314	0.972	364.44	0.542	0.090	0.793	0.867	0.5832	0.5330
1000rpm_50%_SOI=20	28.8	100.11	4.406	1.000	453.15	0.696	0.081	0.681	0.784	0.5155	0.4310
1000rpm_75%_SOI=0	51.2	52.48	2.070	0.288	51.00	0.000	0.166	0.857	0.910	0.6445	0.7867
1000rpm_75%_SOI=4	49.2	60.51	2.104	0.298	69.01	0.031	0.172	0.915	0.948	0.6786	0.7947
1000rpm_75%_SOI=8	60	69.29	1.873	0.228	124.35	0.127	0.170	0.891	0.933	0.6647	0.7481
1000rpm_75%_SOI=12	48.4	78.08	2.698	0.480	242.19	0.331	0.172	0.912	0.946	0.6766	0.6737
1000rpm_75%_SOI=16	47.6	86.85	3.023	0.579	383.22	0.575	0.166	0.860	0.912	0.6460	0.5577
1000rpm_75%_SOI=20	53	93.73	2.772	0.502	427.34	0.651	0.157	0.772	0.852	0.5934	0.4956
1000rpm_100%_SOI=0	116	59.24	1.126	0.000	66.38	0.027	0.233	0.264	0.379	0.2922	0.5647
1000rpm_100%_SOI=4	114.8	68.12	1.125	0.000	89.46	0.067	0.241	0.309	0.432	0.3277	0.5700
1000rpm_100%_SOI=8	112.6	76.93	1.136	0.003	163.57	0.195	0.246	0.335	0.461	0.3472	0.5304
1000rpm_100%_SOI=12	109.4	86.26	1.306	0.055	324.67	0.473	0.247	0.338	0.465	0.3499	0.4206
1000rpm_100%_SOI=16	105.6	95.70	1.669	0.166	409.55	0.620	0.242	0.316	0.439	0.3325	0.3514
1000rpm_100%_SOI=20	104.2	104.45	2.068	0.287	495.32	0.769	0.233	0.265	0.380	0.2925	0.2680
1500rpm_25%_SOI=0	21	47.48	3.686	0.780	57.01	0.010	0.067	0.644	0.754	0.4882	0.6888
1500rpm_25%_SOI=4	21.6	53.86	3.426	0.701	57.91	0.012	0.070	0.697	0.796	0.5209	0.7078
1500rpm _25%_SOI=8	21.6	60.62	3.528	0.732	74.24	0.040	0.071	0.712	0.808	0.5302	0.7021
1500rpm _25%_SOI=12	21.2	67.59	3.887	0.842	125.29	0.129	0.070	0.688	0.789	0.5155	0.6579
1500rpm _25%_SOI=16	23	73.78	3.670	0.776	207.45	0.271	0.067	0.648	0.757	0.4906	0.5861
1500rpm _25%_SOI=20	19.8	79.62	4.354	0.984	266.62	0.373	0.063	0.595	0.714	0.4575	0.5253
1500rpm _50%_SOI=0	29.6	50.92	3.057	0.589	51.26	0.000	0.182	0.849	0.905	0.6452	0.7869
1500rpm _50%_SOI=4	29.6	58.17	3.088	0.598	65.23	0.025	0.188	0.904	0.941	0.6780	0.7969
1500rpm _50%_SOI=8	29.8	66.10	3.232	0.642	89.82	0.067	0.191	0.926	0.955	0.6907	0.7876
1500rpm _50%_SOI=12	30	74.48	3.620	0.760	186.57	0.235	0.189	0.915	0.948	0.6842	0.7167
1500rpm _50%_SOI=16	30.6	82.16	3.739	0.797	323.73	0.472	0.185	0.876	0.923	0.6614	0.6081
1500rpm _50%_SOI=20	31.6	89.26	3.592	0.752	368.62	0.550	0.179	0.822	0.887	0.6291	0.5577
1500rpm _75%_SOI=0	51	53.68	2.065	0.286	55.00	0.007	0.304	0.831	0.893	0.6762	0.8030
1500rpm _75%_SOI=4	51.8	61.45	2.081	0.291	72.27	0.037	0.315	0.894	0.934	0.7142	0.8138
1500rpm _75%_SOI=8	52	70.07	2.217	0.333	124.03	0.126	0.321	0.932	0.959	0.7375	0.7920
1500rpm _75%_SOI=12	52.2	79.00	2.421	0.395	238.01	0.324	0.322	0.940	0.963	0.7419	0.7157
1500rpm _75%_SOI=16	53	87.90	2.643	0.463	380.15	0.569	0.318	0.917	0.949	0.7281	0.6091
1500rpm _75%_SOI=20	55.2	95.33	2.578	0.443	419.10	0.637	0.310	0.867	0.917	0.6980	0.5641
1500rpm _100%_SOI=0	107.4	61.71	1.208	0.025	71.58	0.036	0.424	0.553	0.677	0.5513	0.7166
1500rpm _100%_SOI=4	105.6	70.32	1.229	0.032	94.74	0.076	0.441	0.621	0.735	0.5991	0.7292
1500rpm _100%_SOI=8	105.6	79.04	1.306	0.055	162.92	0.194	0.452	0.661	0.768	0.6271	0.6988
1500rpm_100%_SOI=12	105.6	88.80	1.453	0.100	327.06	0.478	0.456	0.678	0.781	0.6383	0.5919
1500rpm_100%_SOI=16	133.8	98.72	1.339	0.065	472.88	0.730	0.439	0.610	0.727	0.5919	0.4632
1500rpm_100%_SOI=20	109.2	108.35	1.839	0.218	584.72	0.923	0.442	0.625	0.739	0.6022	0.3920
2000rpm_25%_SOI=0	21.4	55.33	3.313	0.667	77.39	0.046	0.093	0.471	0.602	0.3887	0.6149
2000rpm_25%_SOI=4	21.8	59.22	3.147	0.616	73.20	0.038	0.099	0.539	0.665	0.4341	0.6451
2000rpm_25%_SOI=8	22	65.74	3.218	0.638	89.59	0.067	0.102	0.570	0.692	0.4546	0.6461
2000rpm_25%_SOI=12	21.8	72.75	3.445	0.707	116.85	0.114	0.102	0.571	0.693	0.4551	0.6275
2000rpm_25%_SOI=16	25.4	79.04	3.055	0.588	215.97	0.285	0.100	0.547	0.672	0.4396	0.5496
2000rpm_25%_SOI=20	21.2	85.40	3.807	0.817	282.16	0.400	0.097	0.516	0.645	0.4193	0.4916
2000rpm_50%_SOI=0	27.8	55.25	3.281	0.657	64.02	0.023	0.269	0.803	0.874	0.6488	0.7803
2000rpm_50%_SOI=4	27.6	63.12	3.210	0.636	79.23	0.049	0.280	0.873	0.921	0.6912	0.7952
2000rpm_50%_SOI=8	39.4	71.27	2.371	0.380	103.68	0.091	0.280	0.872	0.921	0.6910	0.7781
2000rpm_50%_SOI=12	28.2	80.32	3.663	0.774	205.98	0.268	0.287	0.918	0.950	0.7183	0.7237
2000rpm_50%_SOI=16	28.8	88.82	3.910	0.849	334.32	0.490	0.283	0.891	0.933	0.7023	0.6253
2000rpm_50%_SOI=20	29.4	96.12	3.816	0.820	399.76	0.603	0.276	0.845	0.903	0.6747	0.5635
2000rpm_75%_SOI=0	42.8	58.41	2.640	0.462	67.55	0.029	0.429	0.842	0.900	0.7238	0.8229
2000rpm_75%_SOI=4	41.8	66.55	2.739	0.492	85.98	0.061	0.448	0.926	0.955	0.7763	0.8416
2000rpm_75%_SOI=8	42	74.88	2.836	0.521	116.87	0.114	0.459	0.976	0.986	0.8070	0.8386
2000rpm_75%_SOI=12	42	84.71	3.024	0.579	251.58	0.347	0.464	1.000	1.000	0.8214	0.7541
2000rpm_75%_SOI=16	42.8	94.26	3.231	0.642	410.98	0.623	0.463	0.993	0.996	0.8170	0.6411
2000rpm_75%_SOI=20	45.6	102.35	2.844	0.524	487.74	0.756	0.455	0.956	0.973	0.7945	0.5745
2000rpm_100%_SOI=0	97.2	63.64	1.345	0.067	77.37	0.046	0.587	0.666	0.772	0.6749	0.7867
2000rpm_100%_SOI=4	97.6	72.38	1.393	0.082	100.77	0.086	0.614	0.750	0.836	0.7332	0.8055
2000rpm_100%_SOI=8	98.8	80.85	1.479	0.108	158.71	0.186	0.634	0.812	0.880	0.7751	0.7905
2000rpm_100%_SOI=12	100.8	90.37	1.677	0.168	311.79	0.451	0.646	0.849	0.905	0.8001	0.6996
2000rpm_100%_SOI=16	104.2	101.02	1.622	0.151	510.81	0.796	0.648	0.855	0.909	0.8041	0.5642
2000rpm_100%_SOI=20	111.6	110.71	1.599	0.144	588.82	0.930	0.639	0.828	0.891	0.7862	0.4995
2500rpm_25%_SOI=0	23.2	51.47	2.776	0.503	66.94	0.028	0.123	0.287	0.406	0.2721	0.5522
2500rpm_25%_SOI=4	23.4	55.41	2.756	0.497	64.70	0.024	0.131	0.358	0.487	0.3255	0.5858
2500rpm _25%_SOI=8	23.2	61.64	2.927	0.549	78.68	0.048	0.136	0.401	0.532	0.3564	0.5947

Table A4cont.

Case n (rpm)_Load (%) _SOI°	Combustion duration °CA	Fmax kN	CII_{raw} J/°CA^2	CII_{norm}	MLI_{raw} bar^2/°CA	MLI_{norm}	BP*	BTE*	BSFC*	$Perf_{Score}$	Balanced score
2500rpm _25%_SOI=12	23.2	68.36	3.129	0.611	103.08	0.090	0.138	0.421	0.552	0.3704	0.5862
2500rpm _25%_SOI=16	28	74.57	2.693	0.478	196.68	0.252	0.138	0.417	0.548	0.3677	0.5198
2500rpm _25%_SOI=20	24.6	80.53	3.130	0.611	255.06	0.353	0.136	0.399	0.530	0.3547	0.4716
2500rpm _50%_SOI=0	30	52.75	3.047	0.586	57.63	0.011	0.344	0.690	0.791	0.6085	0.7605
2500rpm _50%_SOI=4	29.4	59.95	3.126	0.610	71.06	0.035	0.361	0.775	0.854	0.6634	0.7841
2500rpm _50%_SOI=8	29.6	67.17	3.280	0.657	92.34	0.072	0.372	0.827	0.890	0.6962	0.7891
2500rpm _50%_SOI=12	30.2	75.37	3.421	0.700	173.31	0.212	0.376	0.847	0.904	0.7093	0.7409
2500rpm _50%_SOI=16	31.2	83.49	3.439	0.705	302.19	0.435	0.375	0.841	0.900	0.7054	0.6494
2500rpm _50%_SOI=20	40	90.18	2.633	0.459	345.55	0.510	0.366	0.797	0.869	0.6773	0.6025
2500rpm _75%_SOI=0	42.6	59.26	2.627	0.458	70.80	0.034	0.530	0.737	0.826	0.6977	0.8049
2500rpm _75%_SOI=4	42.2	67.10	2.659	0.467	88.35	0.065	0.554	0.826	0.889	0.7565	0.8280
2500rpm _75%_SOI=8	41.8	75.22	2.792	0.508	116.97	0.114	0.573	0.891	0.933	0.7991	0.8338
2500rpm _75%_SOI=12	42.2	84.44	2.962	0.560	235.38	0.319	0.583	0.927	0.955	0.8216	0.7654
2500rpm _75%_SOI=16	58.8	93.85	2.265	0.348	387.50	0.582	0.567	0.871	0.920	0.7858	0.6386
2500rpm _75%_SOI=20	47	101.87	2.857	0.528	459.93	0.707	0.576	0.902	0.940	0.8061	0.6007
2500rpm _100%_SOI=0	64.8	68.26	1.944	0.250	94.26	0.075	0.733	0.678	0.781	0.7307	0.8085
2500rpm _100%_SOI=4	62.8	77.34	2.011	0.270	117.65	0.115	0.771	0.777	0.855	0.8011	0.8345
2500rpm _100%_SOI=8	63	86.44	2.127	0.305	158.82	0.187	0.798	0.849	0.905	0.8508	0.8359
2500rpm_100%_SOI=12	63.6	96.01	2.241	0.340	324.79	0.474	0.816	0.894	0.935	0.8817	0.7395
2500rpm_100%_SOI=16	65.2	107.17	2.446	0.403	492.70	0.764	0.822	0.910	0.945	0.8925	0.6298
2500rpm_100%_SOI=20	69	117.64	2.488	0.416	628.94	1.000	0.815	0.893	0.934	0.8806	0.5284
3000rpm_25%_SOI=0	23.2	52.06	2.534	0.430	68.47	0.030	0.106	0.000	0.000	0.0353	0.4091
3000rpm_25%_SOI=4	22.2	55.13	2.667	0.470	65.64	0.025	0.117	0.086	0.137	0.1133	0.4579
3000rpm_25%_SOI=8	22.4	61.06	2.799	0.510	78.49	0.048	0.123	0.133	0.207	0.1545	0.4737
3000rpm_25%_SOI=12	30.6	66.95	2.131	0.307	98.68	0.082	0.121	0.119	0.187	0.1423	0.4524
3000rpm_25%_SOI=16	29.6	72.60	2.307	0.360	180.36	0.224	0.121	0.118	0.186	0.1417	0.3955
3000rpm_25%_SOI=20	26.6	77.92	2.579	0.443	221.80	0.296	0.120	0.106	0.167	0.1309	0.3603
3000rpm_50%_SOI=0	30.6	56.10	3.085	0.597	66.80	0.027	0.429	0.582	0.703	0.5710	0.7317
3000rpm_50%_SOI=4	30.8	63.51	3.088	0.598	81.18	0.052	0.451	0.670	0.775	0.6323	0.7585
3000rpm_50%_SOI=8	30.4	70.72	3.250	0.648	103.42	0.091	0.468	0.738	0.827	0.6778	0.7704
3000rpm_50%_SOI=12	30.6	78.94	3.363	0.682	184.66	0.231	0.478	0.777	0.856	0.7038	0.7298
3000rpm_50%_SOI=16	31	87.44	3.506	0.726	328.02	0.479	0.479	0.782	0.859	0.7066	0.6322
3000rpm_50%_SOI=20	33	94.54	3.224	0.640	382.22	0.573	0.473	0.759	0.842	0.6915	0.5857
3000rpm_75%_SOI=0	51.6	58.03	2.149	0.312	68.57	0.030	0.631	0.572	0.694	0.6324	0.7673
3000rpm_75%_SOI=4	49.8	65.69	2.209	0.330	84.92	0.059	0.669	0.678	0.782	0.7097	0.8024
3000rpm_75%_SOI=8	50	73.08	2.272	0.350	110.78	0.103	0.696	0.755	0.839	0.7632	0.8166
3000rpm_75%_SOI=12	50.2	81.55	2.436	0.400	216.76	0.287	0.715	0.807	0.876	0.7992	0.7648
3000rpm_75%_SOI=16	52.4	90.46	2.523	0.426	387.38	0.582	0.720	0.822	0.887	0.8099	0.6531
3000rpm_75%_SOI=20	57	98.33	2.319	0.364	420.68	0.640	0.714	0.804	0.874	0.7973	0.6225
3000rpm_100%_SOI=0	118	66.75	1.145	0.006	88.76	0.065	0.856	0.410	0.542	0.6030	0.7357
3000rpm_100%_SOI=4	112	75.48	1.197	0.022	111.92	0.105	0.913	0.521	0.649	0.6941	0.7743
3000rpm_100%_SOI=8	110.2	83.60	1.265	0.043	185.34	0.232	0.956	0.605	0.723	0.7613	0.7638
3000rpm_100%_SOI=12	112.4	92.28	1.334	0.064	300.47	0.432	0.984	0.661	0.768	0.8046	0.7101
3000rpm_100%_SOI=16	116.4	102.49	1.393	0.082	508.67	0.792	1.000	0.692	0.793	0.8282	0.5802
3000rpm_100%_SOI=20	125	112.44	1.356	0.070	574.91	0.906	0.997	0.687	0.788	0.8239	0.5318